Engine Impeller Sub-Fragmentation Simulation Using EFG Method

Shoufeng Hu[1], C. T. Wu[2] and Yong Guo[2]

[1]*Hamilton Sundstrand*
One Hamilton Road, M/S 1-3-BC34
Windsor Locks, Connecticut 06096-1010 U.S.A
sam.hu@hs.utc.com

[2]*Livermore Software Technology Corporation*
7374 Las Posita Road, Livermore, CA, 94551 U.S.A
ctwu@lstc.com, yguo@lstc.com

Abstract

Engine impeller burst containment test may lead to the impeller sub-fragmentation. The containment of the impeller debris from sub-fragmentation presents a new challenge, because of the unpredictable pattern of dynamic fracture.

In this study, the capability of EFG failure method in predicting the dynamic fracture of the ductile material, used for the engine impeller under impact loading, is demonstrated. In the EFG method, the combination of fast transformation method and meshfree visibility approach with cohesive fracture is proven to be an efficient way to model the progressive fracture in a general three-dimensional problem. In this study, the Mode-I fracture is adopted and the crack is assumed to propagate cell-by-cell in the direction of maximum principal stress. The meshfree visibility approach is introduced to impose the strong-discontinuity in the meshfree approximation as well as to compute the displacement jump in the initially rigid cohesive model.

1 Introduction

It is required by the customer and the Airworthiness Authorities to perform the engine impeller tri-hub burst containment test as part of new engine certification. The test requires a full containment of all the debris resulting from the impact of the impeller burst. Prior to the test, the impeller is sliced with three cuts in radial direction 120˚ apart and each piece has one-third of the total rotor mass. The cuts are not complete, leaving some material to connect the three rotor segments as "fuses". The "fuses" break at the designated rotor containment speed. The three impeller segments are free to hit the containment components. The success criterion is that the debris on the witness shield outside of the engine, if any, should have minimal kinetic energy.

The explicit finite element code LS-DYNA® has a long history of being used in the aerospace industry to simulate the tri-hub containment test. The simulations not only guarantee the success of the costly containment test, but also help optimize the containment system for minimal cost and weight.

The key to a successful containment simulation is the modeling of the impeller. The hardware of the most tests show that the impeller segments experience broken or severely damaged blades and rim, but the main hub regions show no fracture or significant deformation. The modeling of the impeller based on the test hardware had been very successful.

Recently, a containment test shows that the impeller experiences the sub-fragmentation at the main hub regions during the test, in additional to the damage of the blades and the rim, which leads to the containment test results significantly deviated from the prediction.

Traditional finite element methodology cannot simulate the dynamic crack propagation without the prior knowledge of the crack propagation direction. As a result, the weak link is embedded in the impeller hub as shown in Figure 1a, based on the test hardware. The strength of the weak link is iterated to match the simulated damage of the containment system to the test hardware. Eventually, the weak link based analysis successfully predicts the result of the containment test with the improved containment system.

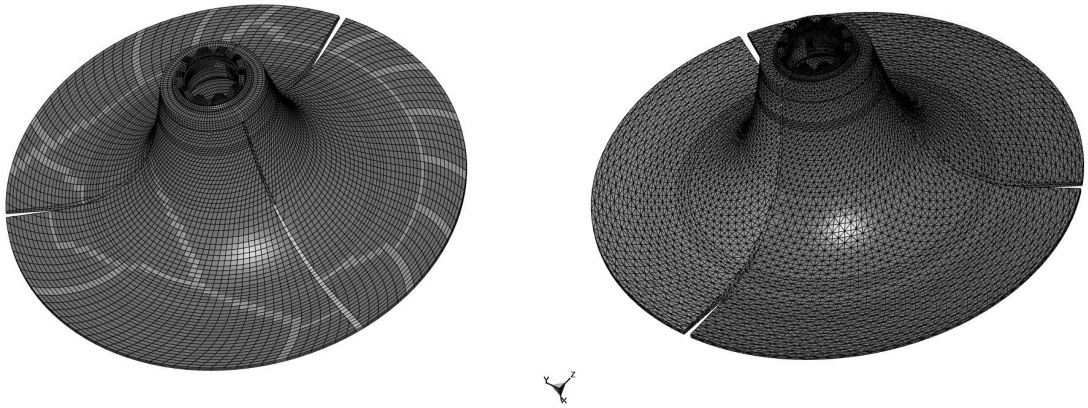

(a) (b)

Figure 1: FEA models of impeller hub for (a) regular hexahedral elements with the weak link and (b) EFG tetrahedral elements

However, there is a clear need for a methodology that can predict the impeller hub sub-fragmentation during the containment simulation without the prior knowledge of the test. Element-Free Galerkin (EFG) method is an ideal candidate for this type of application.

2 EFG Failure Analysis Method

EFG method [1] has demonstrated extraordinary capabilities to solve problems with large deformation, material distortion and moving discontinuities. In the meshfree fracture method, the representation of crack is depicted by the so-called "visibility" criterion [1]. The mid-plane cohesive surface in meshfree domain is shown in Figure 2 and is given by

$$x(\eta) = \sum_{I=1}^{2} \Phi_I^{FEM}(\eta) x_I + \frac{1}{2}\left(\sum_{J \in \Omega_0^+} \Psi_J(X(\eta)) u_J + \sum_{J \in \Omega_0^-} \Psi_J(X(\eta)) u_J \right) \quad (1)$$

where domains on the upper and lower part of the crack are denoted by Ω_0^+ and Ω_0^-, and are defined in the initial configuration. The visibility criterion states that the domain of influence of particles on one side of the crack (i.e. the filled dot in Figure 2) cannot go through the crack surface and the particles on one side of the crack cannot interact with the particles on other side of the crack.

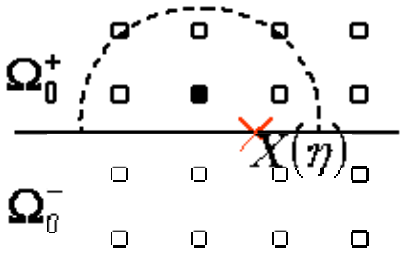

Figure 2: Crack surface is defined by meshfree visibility.

For the kinetics of the crack propagation, the so-called cohesive zone model is adopted to simulate the propagation of the cracks in a continuous body [2] (see Figure 3). Together with the fast transformation method [3], the developed methodology has demonstrated that it is an efficient way to simulate the dynamic fracture problems. Unlike the cohesive element method, with which the cracks can only exist and propagate along the edges or facets between elements, the cracks in EFG failure analysis can propagate in any direction in a three-dimensional media.

In the cohesive zone model, a cohesive constitutive law defines the relation of the traction force to the opening displacement between the crack surfaces, and the initially rigid cohesive law is used in the failure analysis. The linear cohesive law is shown in Figure 3.

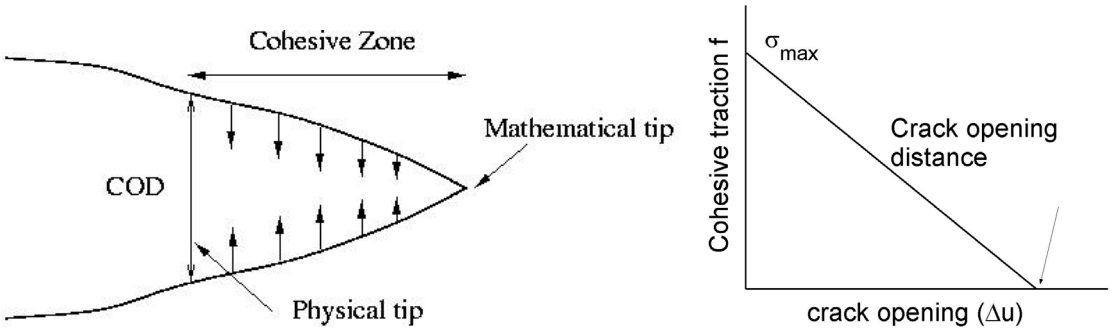

Figure 3: Cohesive zone model and a linear initially rigid cohesive law.

With the initially rigid cohesive law, a crack will initialize and propagate when the maximum tensile principal stress σ_{max} reaches the material ultimate strength. The reason to use the maximum tensile stress criterion for both the crack initiation and crack propagation is to manage the complicated fracture patterns, such as crack branching and crack propagation in complex fracture surfaces. The crack surfaces become traction free if the crack opening displacement exceeds the critical value Δu, which is calculated based on the available traction and the critical energy release rate G_{IC} (or the critical stress intensity factor K_{IC}). However, in our original implementation of the EFG failure method, the crack surface is intrinsic and does not physically exist in the continuous domain. In order to introduce material separation and better handle the interaction between the free crack surfaces, we implement the erosion technique in our method so we can use the self contact algorithm in LS-DYNA® to implement the traction-free crack surfaces. This erosion technique is different from the element erosion method used in the regular finite element failure model and is only activated where the cohesive zone becomes traction free.

2.1 Pressure Smoothing

The cohesive law used in this study describes the relationship of crack opening (known as the displacement jump) and surface traction along the cracked surface. The surface traction is computed at each stress point inside the meshfree computation domain. Since stresses are usually oscillated using the displacement-based Galerkin approach, certain stress smoothing is suggested to provide a better stress calculation in the cohesive law. The following pressure smoothing algorithm is implemented in this study to enhance the performance of the crack propagation in a continuous media.

First, we consider an L_2 projection of pressure in a least-squared sense for each stress point as shown in Figure 4 and given by

$$\Phi(\boldsymbol{P}) = \left\| \boldsymbol{QP} - \frac{\partial \widetilde{W}}{\partial J} \right\|^2_{L_2(\Omega)} \tag{2}$$

or in a discrete form

$$\Theta(\boldsymbol{P}) = \left\| \sum_{j=1}^{3} S_{ij,i} - \psi_{I,j} P_I \right\|^2_{L_2(\Omega)} \tag{3}$$

where $\boldsymbol{P}$ is the coefficient column-vector to be determined at a point of interest; $\boldsymbol{Q}$ is the row-vector that contains a lower-order pressure approximation functions; $\boldsymbol{QP}$ is smoothed pressure; $\frac{\partial \widetilde{W}}{\partial J}$ *or* $S_{ij,i}$ is the pressure directly computed from the displacement field. In Figure 4, all the filled dots are the stress points and the open dot is the one whose smoothed pressure is computed.

Minimization of $\Phi(\boldsymbol{P})$ leads to

$$\widetilde{P} = \boldsymbol{QM}^{-1} \int_\Omega \boldsymbol{Q}^T \frac{\partial \widetilde{W}}{\partial J} d\Omega \quad \textit{where} \quad \boldsymbol{M} = \int_\Omega \boldsymbol{Q}^T \boldsymbol{Q} d\Omega \tag{4}$$

Linearization of the above equation yields the incremental smoothed pressure needed in the computation and is given by

$$\Delta\widetilde{P} = \boldsymbol{QM}^{-1} \int_\Omega \boldsymbol{Q}^T \frac{\partial^2 \widetilde{W}}{\partial J^2} JF_{lk}^{-1} \frac{\partial \Delta u_k}{\partial X_l} d\Omega \tag{5}$$

The smoothed gradient matrix $\widetilde{\boldsymbol{B}}$ associated with the smoothed pressure for the right-hand side becomes

$$\widetilde{\boldsymbol{B}} = \boldsymbol{QM}^{-1} \int_\Omega \boldsymbol{Q}^T \boldsymbol{gB} d\Omega \tag{6}$$

where $\boldsymbol{g}$ is the row vector form of JF_{ij}^{-1} and $\boldsymbol{B}$ is the regular gradient matrix associated with the

deformation gradient constructed using the meshfree approximation.

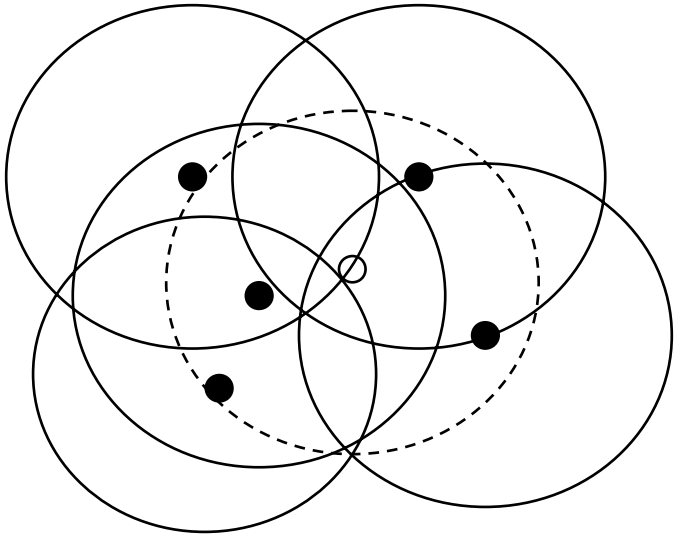

Figure 4: A stress smoothing for the related stress point in meshfree domain.

The new parameter to activate the pressure smoothing is located at the first variable of card 3 in the keyword *SECTION_SOLID_EFG and is described as follows:

***SECTION_SOLID_EFG**

Card 3

Variable	**IPS**	STIME	IKEN	SF	MID	IBR	DS	ECUT
Type	**I**	F	I	F	I	I	F	F
Default	**0**	1.e+20	0	0.0		1	1.01	0.1

IPS = 0 (default) without smoothing;
1 with smoothing.

2.2 Failure Strain Criterion for Ductile Materials

For ductile materials, the strain based failure criterion is often used, which states that the material fails when the maximum effective plastic strain exceeds the material failure strain. To account for this effect in ductile fracture, we add a failure strain criterion to the EFG fracture analysis, in addition to the maximum tensile stress criterion used in the cohesive zone model for crack initiation. With both the failure strain criterion and the maximum tensile stress criterion, a crack will initiate when its effective plastic strain exceeds the material failure strain and the maximum tensile stress exceeds the material tensile strength. The crack propagation direction, however, is determined by the maximum principal tensile stress.

The failure strain can be specified by the 4th variable of card 3 in the keyword *SECTION_SOLID_EFG and is described as follows:

***SECTION_SOLID_EFG**

Card 3

Variable	IPS	STIME	IKEN	**SF**	MID	IBR	DS	ECUT
Type	I	F	I	**F**	I	I	F	F
Default	0	1.e+20	0	**0.0**		1	1.01	0.1

2.3 Cohesive Law for Ductile Materials

Initially, only triangular shaped cohesive law (see Figure 3) is implemented in the EFG failure analysis, which is more suitable to model the brittle crack propagation. In order to simulate crack propagation in ductile materials, the Tvergaard and Hutchinson cohesive model [4] is implemented in this study, as illustrated in Figure 5.

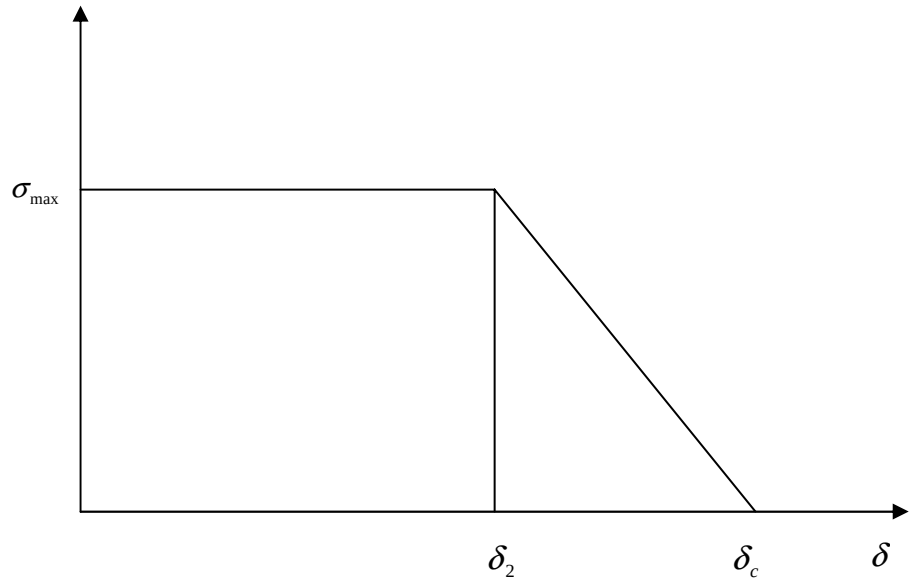

Figure 5: Initially rigid Tvergaard and Hutchinson cohesive law.

The keyword input for this cohesive law is similar as the original cohesive law, with an additional parameter which can be specified by the second variable in card 2 in the keyword *MAT_COHESIVE_TH.

***MAT_COHESIVE_TH**

Card 1

Variable	MID	RO	ROFLG	INTFAIL	SIGMAX	NLS	TLS	
Type	A	F	I	I	F	F	F	
Default			0	1				

Card 2

Variable	LAMDA1	**LAMDA2**	LAMDAF	STFSF				
Type	F	**F**	F	F				
Default	0.0	**0.0**						

$\delta_2 = \frac{2}{3}\delta_c$ is used in this study. If $\delta_2 = 0.0$, this cohesive law changes back to the triangular shaped cohesive law as mentioned initially.

3 Numerical Results

EFG needs no mesh by definition. However, the EFG failure method requires four-noded tetrahedral element as its background mesh to establish the particle associativity. As such, the original hexahedral mesh of the impeller hub, as shown in Figure 1a, is transformed into the tetrahedral mesh, as shown in Figure 1b. The number of nodes in Figure 1a is the same as the number of particles in Figure 1b.

All the other components in the analysis, except the impeller, are kept unchanged as the regular FEA mesh.

The material for impeller is titanium alloy and is modeled by piecewise linear plasticity with strain hardening and strain-rate effect.

The most challenge part in the analysis is to determine the critical strain for crack initiation. If the critical value is set to be low, which leads to the crack early initiation, the impeller hub will erode into numerous small pieces, which is not what happened in the test. If the critical value is set to be high, which leads to the crack late initiation, the impeller hub sub-fragmentation does not occur. Once the crack is initiated, the propagation is governed by the cohesive zone model, based on the test data of K_{IC}.

We do not know the correct value of the failure strain for the titanium alloy which should be used. Based on the material stress-strain curve, the failure strain obtained is about 0.04 at the operating temperature. To study the effect of the failure strain, simulations with three failure strains are tested — 0.01, 0.02 and 0.04.

The numerical results for the failure strain $\varepsilon_f = 0.04$ are shown in Figure 6 and Figure 7, which has better correlation with the test hardware than that from the other two failure strains. The results of the other two failure strains show much more significant sub-fragmentation and erosion of the impeller.

The fracture patterns from the inner and outer views of the sub-fragmented impellers are similar to the test hardware for some pieces (e.g. see Figure 7 impeller piece 2), but not the other pieces. The fragmented pieces in the rim of the impeller erode significantly in the simulation, which does not happen in the test. More importantly, the regular FEA simulation with the impeller weak link successfully simulates the damage of the containment components, but the EFG method does not.

4 Conclusion and Suggested Future Work

Numerical simulation results demonstrate that the current implementation of the EFG failure analysis method can simulate the impeller sub-fragmentation during the containment test. However, more work is needed in order for this technology to have practical significance.

The major problem in current simulation is the balance of the crack initiation and propagation. One of the possible solutions for improvement is to increase the mesh density, or the particle density. After many numerical tests, it is realized that the mesh density, as well as the distribution of the mesh density, can have significant impact on the results. The other possible area of improvement is to use a cohesive law that takes the strain and strain-rate effect into account [5].

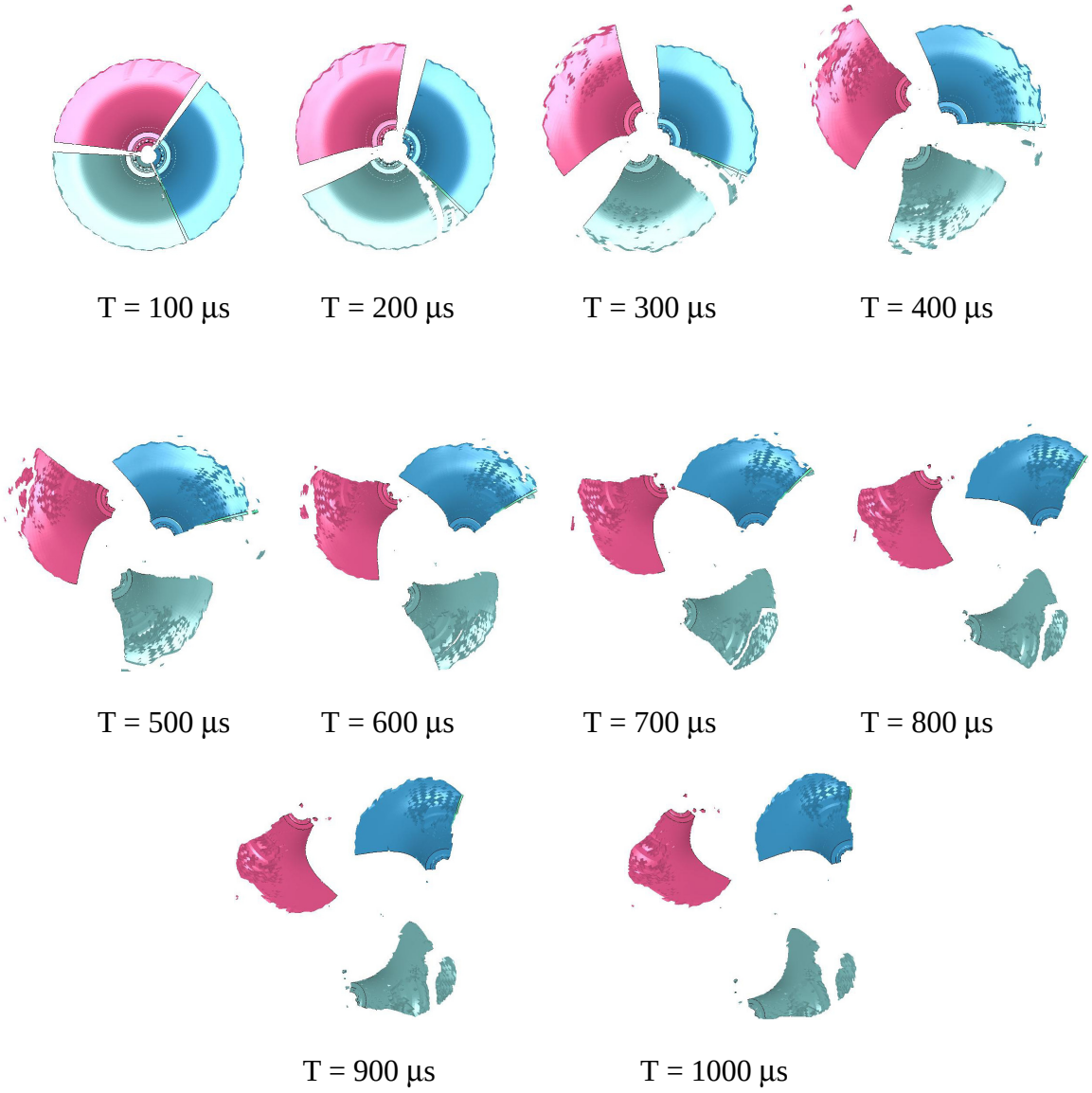

Figure 6: Comparison of the impeller sub-fragmentation at different time.

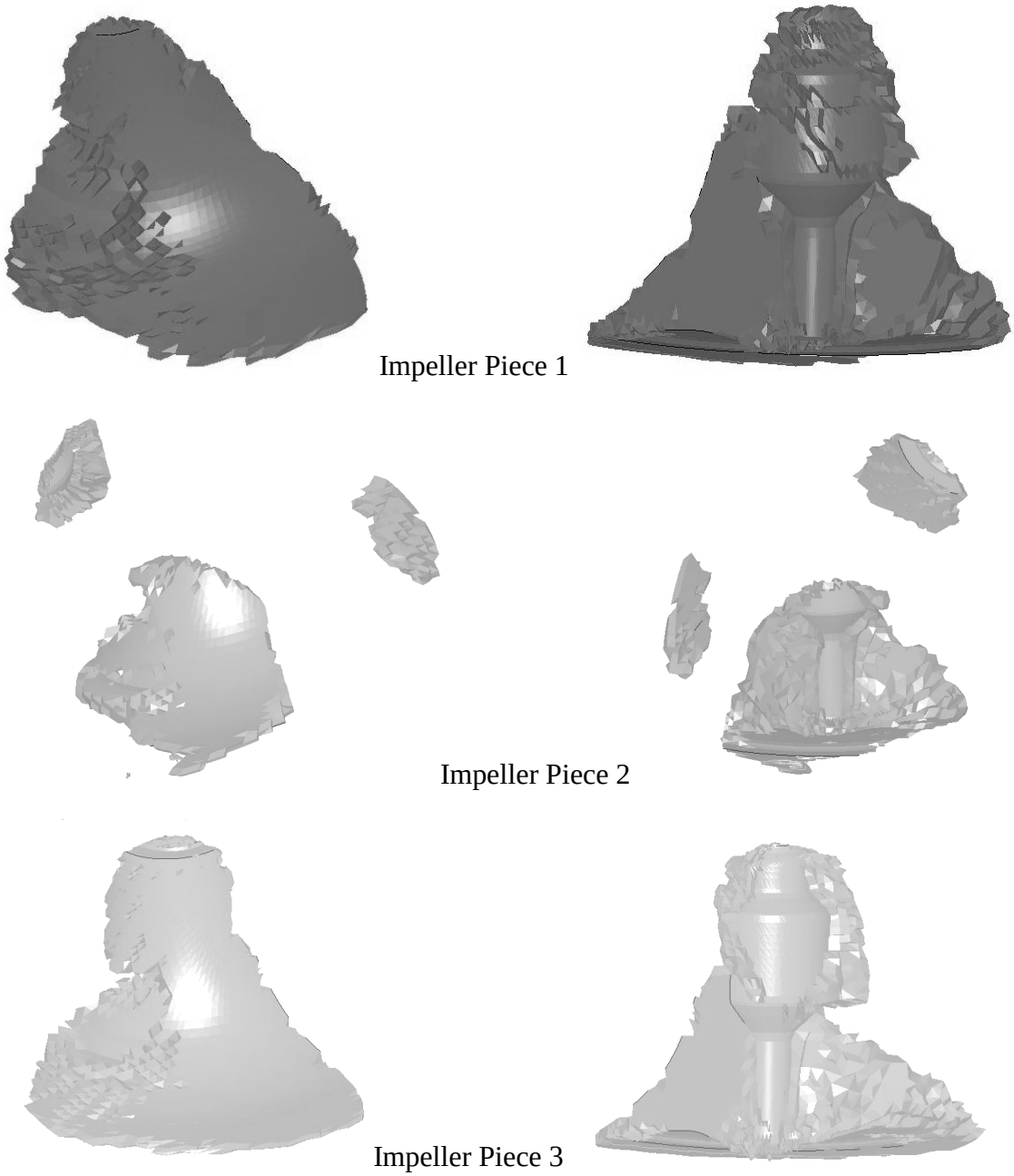

Figure 7: The final shape of the engine impeller fragments with $\varepsilon_f = 0.04$.

References

1. Belytschko, T., Lu Y. Y. and Gu, L., "Crack propagation by element-free Galerkin methods", *Engineering Fracture Mechanics*, V.51, 295-315, 1995.

2. Espimosa, H. D. and Zavattieri, P. D., "A grain level model for the study of failure initiation and evolution in polycrystalline brittle materials. Part I: theory and numerical implementation", *Mechanics of Materials*, V.35, 333-364, 2003.

3. Wu, C. T. and Lu, H. S., "Practical fast meshfree analysis", U.S. Patent, 2009.

4. Tvergaard, V. and Hutchinson, J.W., "The relation between crack growth resistance and fracture process parameters in elastic-plastic solids", *J. Mech. Phys. Solids*, V.40, 1377-1397, 1992.

5. Tvergaard, V. and Hutchinson, J.W., "Effect of strain-dependent cohesive zone model on predictions of crack growth resistance", *Int. J. Solids Structures*, V. 33, 3297-3308, 1996.